processes

MDPI

Review

Elasticity and Viscoelasticity Imaging Based on Small Particles Exposed to External Forces

Hasan Koruk * and Antonios N. Pouliopoulos

Department of Surgical & Interventional Engineering, School of Biomedical Engineering & Imaging Sciences, King's College London, London SE1 7EU, UK; antonios.pouliopoulos@kcl.ac.uk
* Correspondence: hasan.koruk@kcl.ac.uk; Tel.: +44-793-677-8644

Abstract: Particle-mediated elasticity/viscoelasticity imaging has the potential to expand the elasticity imaging field, as it can provide accurate and local tissue elastic properties as well as density and viscosity. Here, we investigated elasticity imaging based on small particles located within the tissue and at the tissue interface exposed to static/dynamic external loads. First, we discuss elasticity/viscoelasticity imaging methods based on the use of particles (bubbles and rigid spheres) placed within the tissue. Elasticity/viscoelasticity imaging techniques based on the use of particles (bubbles, rigid, and soft spheres) located at the tissue interface are then presented. Based on new advances, we updated some of the models for the responses of the particles placed within the tissue and at the tissue interface available in the literature. Finally, we compared the mathematical models for the particles located within the tissue and at the tissue interface and evaluated the elasticity/viscoelasticity imaging methods based on the use of small particles. This review summarized the methods for measuring the elasticity and viscosity of material using particles exposed to external forces. Remote viscoelasticity imaging can be used to improve material characterization in both medical and industrial applications and will have a direct impact on our understanding of tissue properties or material defects.

Keywords: elasticity imaging; elastography; bubble; sphere; interface; mathematical modelling; shear modulus; ultrasound sensors; viscosity; viscoelasticity imaging

Citation: Koruk, H.; Pouliopoulos, A.N. Elasticity and Viscoelasticity Imaging Based on Small Particles Exposed to External Forces. *Processes* **2023**, *11*, 3402. https://doi.org/10.3390/pr11123402

Academic Editors: Vahid Rezania, Harvey Ho and Yuncheng Du

Received: 31 October 2023
Revised: 4 December 2023
Accepted: 7 December 2023
Published: 11 December 2023

1. Introduction

There are various imaging techniques, such as X-ray imaging, ultrasound imaging, magnetic resonance imaging (MRI), and optical imaging, to detect abnormalities [1]. X-ray imaging can provide detection of lesions when they absorb X-ray radiation differently from normal tissue. MRI produces multiplanar imaging and clear soft tissue contrast by differentiating structures based on their water content, etc. Sonography can be used to detect abnormalities due to their hypoechoic or hyperechoic appearance on the B-scan and/or the acoustic shadowing effect they lead to. However, these medical imaging techniques show tissue properties that are typically not related to the distinct mechanical properties of tissue, such as shear modulus and viscosity. The diagnostic value of characterizing the mechanical properties of tissues resulted in the development of methods such as magnetic resonance elastography (MRE) and ultrasound elastography for detecting tissue mechanical properties [2]. In these methods, a static, quasi-static, or dynamic force is applied to the tissue, and the deformation caused by the applied force is detected using a traditional imaging technique such as MRI or ultrasound imaging. Many attempts have been made to develop elasticity imaging methods with distinct capabilities, especially using ultrasound technology [3,4]. Some of these methods include vibro-acoustography [5], shear wave elasticity imaging (SWEI) [6], acoustic radiation force impulse imaging (ARFI) [7], harmonic motion imaging (HMI) [8], supersonic shear imaging (SSI) [9], and shear wave spectroscopy (SWS) [10]. Readers may refer to the review papers for further information about ultrasound-based elasticity imaging methods [11,12] and the clinical use of ultrasound elastography [13–17].

In addition to the aforementioned methods, acoustic radiation force-based elasticity methods that are based on the use of spherical objects (i.e., gas bubbles and rigid spheres) placed within the tissue have been proposed to determine the material's mechanical properties [18–22]. However, in these methods, a high-powered laser is exploited to create a bubble inside the medium. This restricts the application of these techniques to only shallow targets and demands local destruction of the target material [20]. Additionally, there is a need to locate a bubble (or a non-deformable sphere) within the tissue, which may not be allowed in human tissue. A more rational technique based on the use of particles located at the material interface has recently been introduced to determine the viscoelastic properties of soft materials [23,24]. It is worth noting that the acoustic radiation force-based elasticity imaging methods that deform the tissue cause a complicated displacement field [20]. The transducer's focusing characteristics and target geometry affect the displacement field. For these absorption-based techniques, the focal volume affects elasticity reconstruction. On the other hand, for elasticity imaging based on the use of small particles, particle displacement is independent of the transducer's focal zone and is influenced only by the local material's viscoelastic properties. As the object in the elasticity imaging methods based on small particles can be considered as almost a discrete target, simple and accurate elasticity reconstruction can be performed. By exploiting the analytical models for the response of the small particles placed within the medium or at the tissue interface, in addition to the elastic properties of the tissue, the density and viscosity of the material can be determined. It should be noted that parameters such as viscosity can be used as additional biomarkers for the evaluation of materials [25].

Elasticity imaging based on the absorption mechanism and the use of small particles is illustrated in Figure 1. In the elasticity imaging methods based on the absorption mechanism (Figure 1a), displacements vary considerably over the region exposed to the acoustic radiation force because of the differences in the exerted force over the same region. Contrarily, in the elasticity imaging methods based on the use of small particles (Figure 1b), only the displacement of the particle is measured, which can be achieved to align with the focus of the exerted force. Because the radiation force exerted on the particle placed within the material or at the material interface can be much greater than that occurring in a pure absorbing medium, a lower acoustic power can be employed in a moderately attenuating medium for elasticity imaging methods based on small particles. Similar displacements can be achieved with far lower acoustic intensities with particle-based methods. The elasticity imaging methods based on small particles located within the tissue and at the tissue interface have the potential to determine local tissue properties with improved measurement resolution at variable depths.

Particle-mediated elasticity imaging is illustrated in Figure 2. Although the particle is pushed mostly using ultrasound, the excitation force (f_e) can be applied using any other method, such as magnetic or mechanical excitation. Monitoring the displacement of the particle (u) using ultrasound is practical, yet particle imaging can be performed using other methods, such as optical imaging or magnetic resonance imaging. Although there is a need to use a coupling material such as gel or water between the tissue and transducer for ultrasonic excitation, there is no need for a coupling medium (or only air around the medium) for other excitation methods, such as a magnetic force. In addition to the elastic properties of material, the density, Poisson's ratio, and viscosity of material can be identified in elasticity imaging based on small particles. Therefore, instead of using the term elasticity imaging, we suggest using the term viscoelasticity imaging.

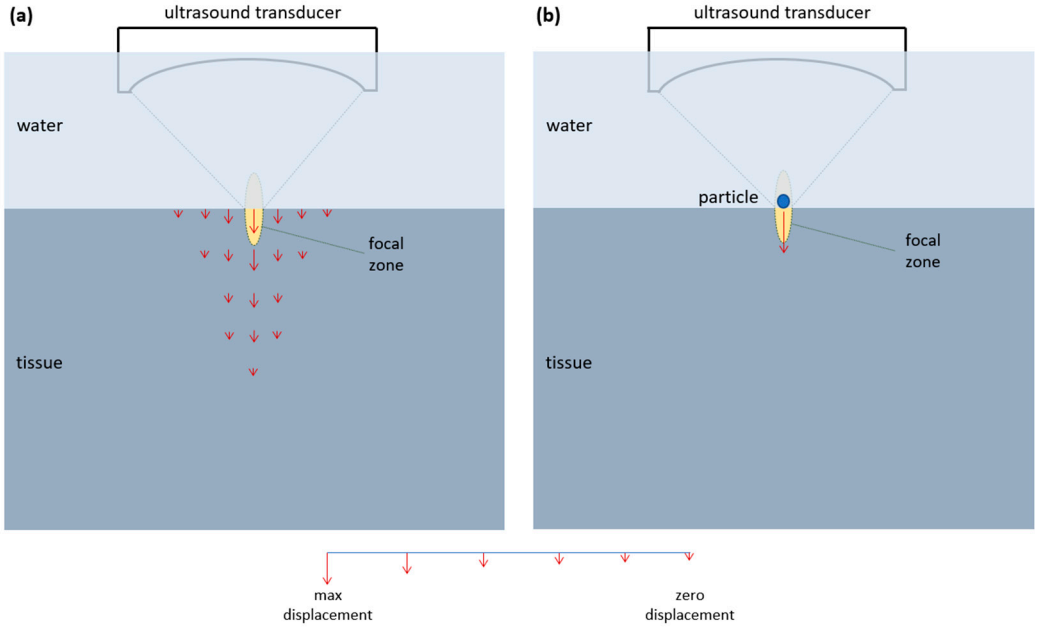

Figure 1. The elasticity imaging based on the absorption mechanism (**a**) and the use of small particles (**b**). The arrows show the displacement produced due to the acoustic radiation force. Displacements vary considerably over the region exposed to the acoustic radiation force because of the differences in the exerted force over the same region for elasticity imaging based on the absorption mechanism. Only the displacement of the particle is measured, which can be managed to align with the focus of the exerted force for elasticity imaging based on small particles.

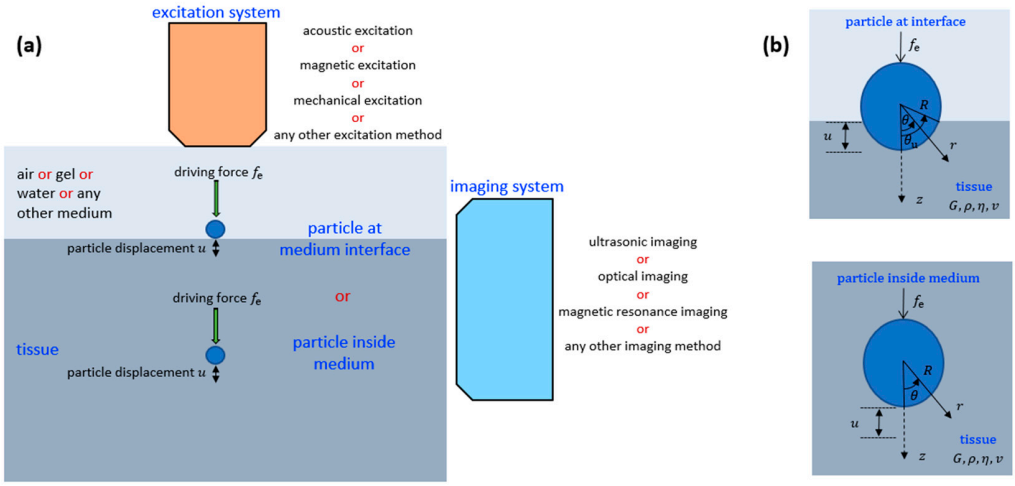

Figure 2. (**a**) Elasticity imaging based on small particles located within the material and at the material interface. Although the particle is pushed mostly using ultrasound, the excitation force (f_e) can be applied using any other method, such as magnetic excitation. Similarly, although monitoring the displacement of the particle (u) using ultrasound is quite practical, the imaging can be performed using other methods, such as optical imaging. (**b**) The schematic for the particle located within the material and at the material interface. G, ρ, η and v show the medium shear modulus, density, viscosity, and Poisson's ratio, respectively, and r and θ show the radial and polar coordinates, respectively.

Although there have been a huge number of research studies (e.g., [26,27]) and some review papers (e.g., [11,12]) on the elasticity imaging techniques based on the absorption mechanism, there have been a limited number of research studies on the particle-mediated elasticity imaging methods. To the best of the authors' knowledge, there is currently no

review study focusing on the elasticity imaging techniques based on the use of small particles located within the tissue and at the tissue interface. We believe that elasticity imaging based on the use of small particles has the potential to change the field, as they can provide the determination of accurate and local tissue elastic properties as well as density and viscosity. Here, we examined the mathematical models for small particles located within the tissue and at the tissue interface. In addition, we compared the mathematical models for small particles located within the tissue and at the tissue interface and provided elasticity/viscoelasticity imaging results based on these models and experiments. This paper is the first review study on elasticity and viscoelasticity imaging based on the use of small (nanometer-, micrometer-, or millimeter-sized) particles (e.g., bubbles and rigid and soft spheres) located within the tissue and at the tissue interface exposed to static and dynamic external forces. Elasticity/viscoelasticity imaging methods based on the use of particles (bubbles and rigid spheres) placed within the tissue are presented in Section 2. Elasticity/viscoelasticity imaging techniques based on the use of particles (bubbles, rigid, and soft spheres) located at the tissue interface are covered in Section 3. It should be noted that the viscoelastic medium was mostly modeled using the Kelvin–Voigt model in the models available in the literature. In this paper, we extended the responses of particles located within the tissue and at the tissue interface and generalized the relations so that, in addition to the Kelvin–Voigt model, any viscoelastic rheological model, such as the Maxwell, standard linear solid, and Kelvin–Voigt fractional derivative models, can be used to simulate the medium. Furthermore, based on the new advances, in this paper, we updated some of the models for the responses of the particles located within the tissue and at the tissue interface available in the literature. The mathematical models for the small particles located within the tissue and at the tissue interface are compared, and the elasticity and viscoelasticity imaging methods based on the use of the particles are assessed in Section 4. Some concluding remarks are given in Section 5.

2. Elasticity/Viscoelasticity Imaging Using Particles Located within the Tissue

2.1. Bubble Located within the Tissue

There are many mathematical models for the radial oscillations of a bubble inside the elastic and viscoelastic media exposed to sound (e.g., [28–30]). However, these models are generally extensions of the well-known Rayleigh–Plesset equation (e.g., [31]) and were proposed for studying the dynamics of bubbles inside the tissue rather than for using them for elasticity imaging. The first important study for the purpose of elasticity imaging using a bubble located within the medium was performed by Ilinskii et al. [19] in 2005. In this model, the radiation pressure on the object is predicted via the integration of the acoustic field in the medium around the object with respect to the target surface. This approach is like the method applied to estimate Stockes' drag of a solid sphere placed inside a viscous, incompressible liquid [32]. Hence, by assuming the elastic medium as homogeneous, isotropic, incompressible, and non-viscous, Ilinskii et al. [19] proposed models for the static and dynamic displacements of a bubble placed within the soft medium in response to acoustic radiation force. The model for an external static force $f_e = f_0$ and elastic medium is given by [19]:

$$u = \frac{f_0}{4\pi G R} \tag{1}$$

where G is the shear modulus of the medium, and R is the radius of the bubble. For a homogeneous isotropic material, the relationship between the Young's modulus and shear modulus is given by $E = 2G(1 + \nu)$. Ilinskii et al. [19] obtained the following equation of motion for the dynamic displacement of a bubble placed within a soft medium exposed to an acoustic radiation force:

$$\underline{u} + \dot{\underline{u}} + \frac{1}{6}\ddot{\underline{u}} + \frac{1}{18}\dddot{\underline{u}} = \underline{f_e} \tag{2a}$$

where

$$\underline{u} = \frac{u(t)}{R} \tag{2b}$$

$$\underline{f_e} = \frac{f_e}{4\pi G R^2} \tag{2c}$$

$$\underline{t} = \frac{t\sqrt{G/\rho}}{R} \tag{2d}$$

Here, ρ is the density of the material, and t shows the time. The solution to Equation (2a) provides the relationship between the dynamic force and displacement for a bubble placed within the soft elastic medium. The solution of Equation (2a) can be determined analytically (e.g., using the Laplace transformation) or numerically. Readers can refer to the reference [19] to see the details of the derivations of the models (i.e., Equations (1) and (2a)). For a homogeneous, incompressible, and isotropic material, a model was proposed to predict the dynamic response of a bubble placed within the soft viscoelastic material exposed to an acoustic radiation force. The equation correlating the displacement of the bubble placed within the viscoelastic material and the dynamic force is [19]:

$$4\pi(G - j\omega\eta)RU\left(1 - jkR - \frac{1}{6}k^2R^2 + \frac{1}{18}jk^3R^3\right) = F_e \tag{3}$$

where η is the viscosity of the medium, $k = \frac{\omega}{\sqrt{(G-j\omega\eta)/\rho}}$ is the complex wave number of the shear wave with frequency ω, $j = \sqrt{-1}$, F_e is the Fourier transform of the external force $f_e(t)$, and U is a spectral component of the bubble displacement $u(t)$. Readers can refer to the reference [19] to see the details for the derivation of the model (i.e., Equation (3)). The response to a rectangular pulse, characterized by an amplitude f_0 and a duration τ, resembles the impulse response when τ is small and step response when τ is large ($0 \leq t \leq \tau$). The external force is assumed to be a rectangular pulse here; note that the Fourier transform of a rectangular pulse is $F_e = -\frac{jf_0}{\omega}\left(e^{j\omega\tau} - 1\right)$. In conclusion, we can calculate the dynamic displacement of the bubble located within the soft viscoelastic material using the inverse Fourier transformation [33]:

$$u(t) = -\frac{jf_0}{24\pi^2 R}\int_{-\infty}^{\infty} \frac{\left(e^{j\omega\tau} - 1\right)(3 - jkR)e^{-j\omega t}}{\omega(G - j\omega\eta)\left(1 - jkR - \frac{1}{6}k^2R^2 + \frac{1}{18}jk^3R^3\right)}\mathrm{d}\omega \tag{4}$$

We can divide the duration into N points and repeat the calculations over the entire period of interest to numerically determine the dynamic response of the bubble placed within the material using Equation (4).

Exploiting the static model (i.e., Equation (1)), Erpelding et al. [20] identified the Young's moduli of gelatin phantoms. For this purpose, individual bubbles were created by laser-induced optical breakdown. A two-element confocal ultrasonic transducer was used to exert acoustic radiation force on individual bubbles (1.5 MHz) and monitor their displacement within the medium (7.44 MHz). Maximum bubble displacements were used to identify the Young's moduli of different gel phantoms; their Young's moduli were identified to be 1.7–4.8 kPa for the 5–9% gel concentration. Erpelding et al. [34] used the same method to map age-related elasticity changes in porcine lenses. Hollman et al. [35] exploited the same approach to map elasticity in human lenses. Young's modulus varied from 5.2 kPa in the center to 1.1 kPa on the periphery for middle-age lenses. Young's modulus varied from 10.6 kPa in the center to 1.4 kPa on the periphery for old-age lenses. Similarly, Mikula et al. [36] exploited this simple model to determine corneal elasticity. For this purpose, a femtosecond laser-generated microbubble was pushed using a low-frequency and high-intensity acoustic force. The position of the microbubble within the *ex vivo* human cornea was detected using high-frequency and low-intensity ultrasound. The Young's moduli of the central anterior and posterior corneas were determined to be 1.39 and 0.71 kPa, respectively. In another study, using the same technique, Mikula et al. [37] determined the elasticity map across the *ex vivo* human cornea.

Using the dynamic model presented above, Yoon et al. [38] estimated the mechanical properties of gelatin phantoms using a laser-induced microbubble within the phantoms exposed to ultrasound (3.5 MHz). The motion of the microbubble was detected using an imaging transducer (25 MHz). By using both the maximum displacements and the times of maximum displacement of the bubbles, the Young's modulus of the 3% gelatin phantom was determined to be 4.37 ± 0.26 kPa. In another study, exploiting the same model, the Young's moduli and viscosities of *ex vivo* bovine and porcine crystalline lenses were identified using the time characteristics of the microbubble deformation [39].

In the model presented above (i.e., Equations (3) and (4)), the viscoelastic sample was modeled using the Kelvin–Voigt model. In this paper, we extended the response of a bubble located within the soft viscoelastic material and generalized the relations so that, in addition to the Kelvin–Voigt model, any viscoelastic rheological model, such as the Maxwell, standard linear solid, and Kelvin–Voigt fractional derivative models, can be used to simulate the medium. In conclusion, the generalized model for the response of a bubble located within the soft viscoelastic material can be represented as:

$$u(t) = -\frac{jf_0}{24\pi^2 R}\int_{-\infty}^{\infty} \frac{\left(e^{j\omega\tau}-1\right)(3-jkR)e^{-j\omega t}}{\omega G^*\left(1-jkR-\frac{1}{6}k^2R^2+\frac{1}{18}jk^3R^3\right)}\mathrm{d}\omega \tag{5}$$

where $G^*(\omega) = G'(\omega) - jG''(\omega)$ is the complex modulus of the medium material; $G'(\omega)$ and $G''(\omega)$ represent the storage and loss moduli, respectively. Readers may refer to the reference [22] for the expressions of $G'(\omega)$ and $G''(\omega)$ for different rheological models.

2.2. Sphere Located within the Tissue

The response of a spherical object placed within the medium has been studied for over 70 years. Oestreicher [40] obtained the mechanical impedance of an oscillating sphere inside a viscoelastic medium in the frequency domain by modeling the medium using the Kelvin–Voigt model. Chen et al. [18] used the measured response of a vibrating sphere inside a gelatin phantom exposed to modulated ultrasound and the model in the reference [40] for the determination of the material's viscoelastic properties. However, the first important study for the purpose of elasticity imaging using a sphere located within the medium was performed by Ilinskii et al. [19] in 2005. By assuming the elastic medium as homogeneous, isotropic, incompressible, and non-viscous, Ilinskii et al. [19] proposed models for the static and dynamic displacements of a non-deformable sphere located within the medium exposed to acoustic radiation force. The model for a static force f_0 and elastic medium is given by [19]:

$$u = \frac{f_0}{6\pi GR} \tag{6}$$

For a dynamic force f_e and an elastic medium, they obtained the following equation of motion [19]:

$$\underline{u} + \dot{\underline{u}} + \frac{1}{9}\left(1+2\frac{\rho_s}{\rho}\right)\ddot{\underline{u}} = \underline{f_e} \tag{7a}$$

where

$$\underline{u} = \frac{u(t)}{R} \tag{7b}$$

$$\underline{f_e} = \frac{f_e}{6\pi GR^2} \tag{7c}$$

$$\underline{t} = \frac{t\sqrt{G/\rho}}{R} \tag{7d}$$

Here, ρ_s is the density of the sphere. The solution of Equation (7a) gives the relationship between the dynamic force and displacement for a sphere located within the elastic medium. The solution of Equation (7a) can be determined analytically (e.g., using the

Laplace transformation) or numerically. Readers can refer to the reference [19] to see the details of the derivations of the models (i.e., Equations (6) and (7a)). For a homogeneous, isotropic, and incompressible medium, Aglyamov et al. [21] developed a model to predict the dynamic response of a sphere placed within the viscoelastic material exposed to an acoustic radiation force in 2007. The equation relating the displacement of the sphere placed within the viscoelastic medium and the dynamic force is [21]:

$$-m_s\omega^2 U + 6\pi(G - j\omega\eta)RU\left(1 - jkR - \frac{1}{9}k^2R^2\right) = F_e \tag{8}$$

where $m_s = \frac{4}{3}\pi R^3\rho_s$ is the mass of the sphere. Readers can refer to the reference [21] to see the details for the derivation of the model (i.e., Equation (8)). By performing some operations, the dynamic displacement of the sphere located within the viscoelastic material can be found using [33]:

$$u(t) = -\frac{jf_0}{12\pi^2 R}\int_{-\infty}^{\infty}\frac{\left(e^{j\omega\tau} - 1\right)e^{-j\omega t}}{\omega\left[-\frac{2}{9}R^{2\rho_s}\omega^2 + (G - j\omega\eta)\left(1 - jkR - \frac{1}{9}k^2R^2\right)\right]}\mathrm{d}\omega \tag{9}$$

Chen et al. [18], exploiting the measured response of a vibrating sphere inside a gelatin phantom excited by modulated ultrasound and the expression for the mechanical impedance of a vibrating sphere inside the gelation phantom, determined the viscoelastic material properties of gelatin. Karpiouk et al. [41] used the dynamic model presented above for a sphere inside the material to identify the shear modulus of the gelatin phantom. For this purpose, a rigid sphere placed inside the elastic medium was pushed using a short pulse produced by a focused ultrasound transducer (1.5 MHz), and the displacement of the sphere was detected using another focused ultrasound transducer (25 MHz). They determined the shear modulus of the gelatin phantom using the maximum displacement of the sphere and the time required for the rigid sphere to reach the maximum displacement (no need to know the applied force). Using a similar test setup, Shih et al. [42] exploited the spatiotemporal behavior of the sphere displacement and determined the viscoelastic properties of porcine clot (with different hematocrits). The shear modulus of the blood clot was identified to be 585 ± 127 Pa at plasma (and 168 ± 26 Pa at 40% hematocrit). The viscosity of the blood clot was determined to be 0.125 ± 0.025 Pa·s at plasma (and 0.28 ± 0.12 Pa·s at 40% hematocrit). Similarly, Huang et al. [43], by using the dynamic model, identified the shear modulus and viscosity of porcine blood clots based on the spatiotemporal displacement profile of the sphere.

It should be noted that the medium was modeled using the Kelvin–Voigt model in the model presented above (i.e., Equations (8) and (9)). Urban et al. [22] extended the vibration response of a sphere located within the viscoelastic medium and generalized the relations so that, in addition to the Kelvin–Voigt model, any viscoelastic rheological model, such as the Maxwell, standard linear solid, and Kelvin–Voigt fractional derivative models, can be used to simulate the medium. In conclusion, the generalized model for the vibration response of a sphere placed within the viscoelastic material can be represented as:

$$u(t) = -\frac{jf_0}{12\pi^2 R}\int_{-\infty}^{\infty}\frac{\left(e^{j\omega\tau} - 1\right)e^{-j\omega t}}{\omega\left[-\frac{2}{9}R^{2\rho_s}\omega^2 + G^*\left(1 - jkR - \frac{1}{9}k^2R^2\right)\right]}\mathrm{d}\omega \tag{10}$$

Readers may refer to the reference [22] for the expressions of $G^*(\omega) = G'(\omega) - jG''(\omega)$ for different rheological models. Urban et al. [22] determined the viscoelastic properties of gelatin and rubber phantoms by matching the measured and theoretically predicted responses of the spheres inside phantoms using different rheological models for the medium.

It should be noted that the particle located within the tissue has been mostly pushed using acoustic excitation (e.g., [22,41]). However, the particle can be pushed using any proper excitation technique, such as a magnetic force. Recently, Levy and Oldenburg [44]

used magnetic force to excite a sphere inside the medium for elasticity imaging purposes. They formulated the motion of a magnetic particle exposed to the special magnetomotive ultrasound driving force in the frequency domain and then obtained an analytical expression by using the inverse Fourier transform as follows:

$$u(t) = \frac{f_0}{6\pi GR}\left[1 - \frac{1}{\sqrt{\chi^2+\psi^2}}\cos(\omega_0 t - \phi_s) + \omega_0^2 e^{-\omega_b t}\frac{\sqrt{Z^2+1}}{\sqrt{X^2+Y^2}}\cos(\omega_a t - \phi_t)\right] \quad (11)$$

where f_0 and ω_0 are the amplitude and frequency of the driving force, respectively. Readers may refer to the reference [44] for the explanation and expressions of the parameters ω_a, ω_b, χ, ψ, X, Y, ϕ_s and ϕ_t.

In another study, Cebrecos et al. [45] evaluated the complex shear modulus of gelatin by applying a magnetic force to a sphere inside the medium. Because generating an ideal rectangular waveform for the current is not possible (due to the inductance of the coil), the magnetic force was assumed to be a trapezoidal pulse with a rise time t_r. The Fourier transform of this force is $F_e = -\frac{jf_0}{t_r\omega^2}\left(e^{j\omega\tau}-1\right)\left(e^{j\omega t_r}-1\right)$. Hence, the displacement of the sphere located within the material can be found using:

$$u(t) = -\frac{jf_0}{12\pi^2 R t_r}\int_{-\infty}^{\infty}\frac{\left(e^{j\omega\tau}-1\right)\left(e^{j\omega t_r}-1\right)e^{-j\omega t}}{\omega^2\left[-\frac{2}{9}R^2\rho_s\omega^2 + (G-j\omega\eta)\left(1-jkR-\frac{1}{9}k^2R^2\right)\right]}d\omega \quad (12)$$

A 3 MHz ultrasound probe was used to detect the displacement of the sphere. Using the measured response and the theory (i.e., Equation (12)), the shear moduli and viscosities of two different gelatin phantoms were determined as 1.86 ± 0.005 and 4.96 ± 0.025 kPa and 0.61 ± 0.01 and 1.05 ± 0.03 Pa·s, respectively.

3. Elasticity/Viscoelasticity Imaging Using Particles Located at the Tissue Interface

3.1. Bubble Located at the Tissue Interface

Although there are many mathematical models for the radial oscillations of a bubble inside the elastic and viscoelastic media exposed to sound (e.g., [28–31]) and some studies on elasticity imaging based on the use of a bubble located within the elastic and viscoelastic media (e.g., [19,20,34,35]), there are a few studies on the responses of the bubbles placed at the medium interfaces [24,46,47]. Considering the elastic medium as homogeneous, isotropic, incompressible, and non-viscous, Koruk and Choi [46] proposed models for the static and dynamic displacements of a bubble placed at the soft medium interface exposed to an external force in 2018. The model for an external static force $f_e = f_0$ and a soft elastic medium is [46]:

$$u = \frac{f_0}{2\pi GR\left[1-\left(1-\frac{u}{R}\right)^3\right]} \quad (13)$$

For a dynamic force f_e and a soft elastic medium, they obtained the following equation of motion [46]:

$$\underline{u} + \dot{\underline{u}} + \frac{1}{6}\ddot{\underline{u}} + \frac{1}{18}\dddot{\underline{u}} = \underline{f_e} \quad (14a)$$

where

$$\underline{u} = \frac{u(t)}{R} \quad (14b)$$

$$\underline{f_e} = \frac{f_e}{2\pi GR^2(1-\cos^3\theta_u)} \quad (14c)$$

$$\underline{t} = \frac{t\sqrt{G/\rho}}{R} \quad (14d)$$

where θ_u is the angle corresponding to the displacement u (see Figure 2b). The solution of Equation (14a) gives the relationship between the dynamic force and displacement for a bubble placed at the soft elastic material interface. The solution of Equation (14a) can be determined numerically. Readers can refer to the reference [46] to see the details for the derivations of the models (i.e., Equations (13) and (14a)). Later, Koruk and Choi [47], considering the medium as homogeneous, isotropic, and incompressible, proposed a model to predict the dynamic response of a bubble placed at the soft viscoelastic material interface in response to an external force in 2019. The frequency-domain equation relating the displacement of the bubble placed at the soft viscoelastic material interface and the dynamic force can be written as:

$$2\pi(G - j\omega\eta)RU\left(1 - \cos^3\theta_u\right)\left(1 - jkR - \frac{1}{6}k^2R^2 + \frac{1}{18}jk^3R^3\right) = F_e \tag{15}$$

In conclusion, the dynamic displacement of the bubble placed at the soft viscoelastic material interface in response to a rectangular pulse input can be calculated using the inverse Fourier transformation [47]:

$$u(t) = -\frac{jf_0}{12\pi^2R\left\{1 - \left[1 - \frac{u(t)}{R}\right]^3\right\}}\int_{-\infty}^{\infty}\frac{\left(e^{j\omega\tau} - 1\right)(3 - jkR)e^{-j\omega t}}{\omega(G - j\omega\eta)\left(1 - jkR - \frac{1}{6}k^2R^2 + \frac{1}{18}jk^3R^3\right)}\mathrm{d}\omega \tag{16}$$

Readers can refer to the references [46,47] to see the details for the derivation of the model (i.e., Equations (15) and (16)).

Koruk et al. [23] emitted ultrasound pulses across a wall-less channel of gelatin filled with a cloud of microbubbles. The microbubble cloud exposed to ultrasound caused the deformation of the gelatin phantom. The velocity of the shear wave propagated away from the sonicated region was exploited to identify the Young's moduli of the gelatin phantoms ($v_s = \frac{E}{3\rho}$; ρ being the gel density). Hence, they found E = 0.46 ± 0.06 kPa and E = 1.54 ± 0.32 kPa for the 2.5 and 5% gelation phantoms, respectively. Bezer et al. [24] administered individual microbubbles into a wall-less hydrogel tunnel exposed to ultrasound (1 MHz) and tracked the motion of each microbubble using a high-speed camera. Using the mathematical model explained above (i.e., Equation (16)) and the measured response of each microbubble located at the gel interface, they evaluated the Young's moduli (2–8.7 kPa) and the viscosities (0.12–0.20 Pa·s) of the hydrogels.

In the model presented above (i.e., Equations (15) and (16)), the soft viscoelastic material was modeled using the Kelvin–Voigt model. In this paper, we extended the response of a bubble placed at the soft viscoelastic material interface and generalized the relations so that, in addition to the Kelvin–Voigt model, any viscoelastic rheological model, such as the Maxwell and Kelvin–Voigt fractional derivative models, can be used to simulate the medium. The generalized model for the response of a bubble placed at the soft viscoelastic material interface can be represented as:

$$u(t) = -\frac{jf_0}{12\pi^2R\left\{1 - \left[1 - \frac{u(t)}{R}\right]^3\right\}}\int_{-\infty}^{\infty}\frac{\left(e^{j\omega\tau} - 1\right)(3 - jkR)e^{-j\omega t}}{\omega G^*\left(1 - jkR - \frac{1}{6}k^2R^2 + \frac{1}{18}jk^3R^3\right)}\mathrm{d}\omega \tag{17}$$

Readers may refer to the reference [22] for the expressions of $G^*(\omega) = G'(\omega) - jG''(\omega)$ for different rheological models.

3.2. Sphere Located at the Tissue Interface

The displacement of a non-deformable sphere placed at the material interface exposed to a static force can be predicted using the well-known Hertz Model. However, the Hertz model can produce accurate estimates when the ratio of the sphere displacement to the sphere diameter is less than 0.05 [48]. Some extended Hertz models have been developed for more accurate estimates of static loading (e.g., [49–52]). Koruk [53] proposed a Hertz

model for the small and large displacements of a sphere and a Poisson's ratio of v = 0.45 given by:

$$f_0 = \left[\frac{1-0.1\frac{u}{R}}{1+0.5\left(1-0.1\frac{u}{R}\right)}\right]^{3/2}\frac{4E\sqrt{R}}{3(1-v^2)}u^{3/2} \text{ for } v = 0.45 \tag{18}$$

Koruk [54] recently developed a modified Hertz model based on the finite element analyses for the small and large displacements of a sphere and different values of the Poisson's ratio of the medium given below:

$$f_0 = \left\{\frac{1-(v-0.35)\frac{u}{R}}{1+0.5\left[1-(v-0.35)\frac{u}{R}\right]}\right\}^{3/2}\frac{4E\sqrt{R}}{3(1-v^2)}u^{3/2} \tag{19}$$

Among the many investigated models, this was shown to be a more accurate model to accurately estimate the small and large sphere displacements (i.e., $\frac{u}{R} = 0-0.6$) and practical values of the medium Poisson's ratio (i.e., v = 0.30–0.49).

Using the force-displacement relation in Equation (18) and considering the damping of the oscillations of the sphere arising from the radiation of shear waves, Koruk [53] obtained an analytical model to predict the dynamic response of a rigid sphere placed at the elastic material interface. However, as stated before, the force-displacement relation in Equation (19) was shown to produce more accurate estimates. Therefore, the analytical model for the dynamic response of a rigid sphere placed at the elastic material interface in response to a rectangular pulse input in the reference [53] was updated using the force-displacement relation in Equation (19), and the solution is presented in this paper. Hence, the solution is obtained as follows:

$$u(t) = \frac{f}{k} - \frac{f}{k\sqrt{1-\zeta^2}}e^{-\zeta\omega_n t}\cos(\omega_d t - \varphi) \text{ for } 0 \le t \le \tau \tag{20a}$$

$$u(t) = \frac{fe^{-\zeta\omega_n t}}{k\sqrt{1-\zeta^2}}\left\{e^{\zeta\omega_n \tau}\cos[\omega_d(t-\tau)-\varphi] - \cos(\omega_d t - \varphi)\right\} \text{ for } t > \tau \tag{20b}$$

where

$$k = \left[1-(v-0.35)\frac{\delta}{R}\right]1.5\left(\frac{4E^*\sqrt{R}}{3}\right)^{2/3}f_0^{1/3} \tag{20c}$$

$$c = \frac{1}{2}\left(0.5+\frac{\delta}{R}\right)\left(\sqrt{\frac{\rho}{G}}R\right)\left[1-(v-0.35)\frac{\delta}{R}\right]1.5f_0^{1/3}\left(\frac{4E^*\sqrt{R}}{3}\right)^{2/3} \tag{20d}$$

$$m = \frac{1}{3}\pi R^3\left(4\rho_s + \frac{\delta}{R}\rho\right) \tag{20e}$$

$$f = \left\{1+0.5\left[1-(v-0.35)\frac{\delta}{R}\right]\right\}f_0 \tag{20f}$$

$$\omega_n = \sqrt{\frac{k}{m}} \tag{20g}$$

$$\omega_d = \omega_n\sqrt{1-\zeta^2} \tag{20h}$$

$$\zeta = \frac{c}{c_{cr}} = \frac{c}{2\sqrt{km}} \tag{20i}$$

$$\varphi = \tan^{-1}\frac{\zeta}{\sqrt{1-\zeta^2}} \tag{20j}$$

$$\delta = \left(\frac{3f_0}{4E^*\sqrt{R}}\right)^{2/3} \tag{20k}$$

Here, E^* is the reduced Young's modulus of the sphere at the interface of a flat medium with a Young's modulus E and Poisson's ratio ν. For a non-deformable sphere, the reduced Young's modulus is $E^* = E/(1-\nu^2)$. Koruk et al. [55,56] pushed a spherical object placed at the interface of a gelatin phantom using a magnetic force. Using a high-speed camera, the sphere was tracked as it pushed against the gelatin phantom. For example, using the mathematical model explained above (i.e., Equations (20a) and (20b)) and the measured response of the sphere placed at the gelatin-phantom interface, the shear moduli of some gelatin phantoms were determined to be 1.5–2.8 kPa [55]. By using an equivalent viscous damping ratio for the gelatin phantom in the model (i.e., Equations (20a) and (20b)), the equivalent viscous damping ratios of the gelatin phantoms were determined to be 0.12–0.38 [55].

Later, Koruk [54], by using the force-displacement relation in Equation (19) and considering the medium viscosity via the Kelvin–Voigt model, updated the model for the dynamic response of a non-deformable sphere placed at the medium interface in the reference [53]. Overall, the dynamic response of a spherical object placed at the viscoelastic material interface in response to a rectangular pulse input in the frequency domain was determined to be:

$$U = \frac{\left\{1+0.5\left[1-(v-0.35)\frac{\delta}{R}\right]\right\}\left[-\frac{jf_0}{\omega}\left(e^{j\omega\tau}-1\right)\right]}{\frac{1}{3}\pi R^3\left(4\rho_s+\frac{\delta}{R}\rho\right)(-\omega^2)+\left[\frac{1}{2}\left(0.5+\frac{\delta}{R}\right)\left(\sqrt{\frac{\rho}{G-j\omega\eta}}R\right)(-j\omega)+1\right]\left[1-(v-0.35)\frac{\delta}{R}\right]1.5f_0^{1/3}\left(\frac{4\widetilde{E}^*\sqrt{R}}{3}\right)^{2/3}} \tag{21}$$

where $\widetilde{E}^* = 2(G-j\omega\eta)(1+\nu)/(1-\nu^2)$ for a homogeneous isotropic material and a non-deformable sphere. The response of the sphere placed at the viscoelastic material interface in time dmain was obtained using the inverse Fourier transform as follows [54]:

$$u(t) = \frac{1}{2\pi}\int_{-\infty}^{\infty} \frac{\left\{1+0.5\left[1-(v-0.35)\frac{\delta}{R}\right]\right\}\left[-\frac{jf_0}{\omega}\left(e^{j\omega\tau}-1\right)\right]e^{-j\omega t}}{\frac{1}{3}\pi R^3\left(4\rho_s+\frac{\delta}{R}\rho\right)(-\omega^2)+\left[\frac{1}{2}\left(0.5+\frac{\delta}{R}\right)\left(\sqrt{\frac{\rho}{G-j\omega\eta}}R\right)(-j\omega)+1\right]\left[1-(v-0.35)\frac{\delta}{R}\right]1.5f_0^{1/3}\left(\frac{4\widetilde{E}^*\sqrt{R}}{3}\right)^{2/3}}\mathrm{d}\omega \tag{22}$$

In addition to the elastic properties of the medium and size of the sphere, this model includes the corrected models for the inertia force due to the medium involved in motion, the inertia force of the sphere, and the damping due to the oscillations of the sphere arising from the radiation of shear waves. The force-displacement relation is valid for the small and large displacements of the sphere and the practical values of the medium Poisson's ratio. Therefore, the model given above (i.e., Equations (21) and (22)) is considered the most comprehensive mathematical model for the response of a sphere placed at the medium interface in the literature. The mathematical model presented above (i.e., Equations (21) and (22)) can be extended for the response of a soft spherical object placed at the material interface by using the reduced Young's modulus $\widetilde{E}^* = \left[\frac{1-v_1^2}{E_1}+\frac{1-v_2^2}{E_2}\right]^{-1}$ where E_1 and E_2 and v_1 and v_2 show the Young's moduli and Poisson's ratios of the medium and deformable sphere, respectively. Furthermore, the model can be extended for a sphere placed at a spherical interface by replacing R with the relative radius $R^* = \left[\frac{1}{R_1}+\frac{1}{R_2}\right]^{-1}$ where R_1 and R_2 show the radii of the spherical interface and sphere, respectively.

It should be noted that the particles, such as non-deformable spherical objects, are commonly used in conventional indentation tests [57,58] and AFM, or atomic force microcopy [59], to identify the material properties. However, a sphere is attached to a rigid holder in conventional indentation tests and to a flexible beam in AFM. Usually, only the Young's modulus of the sample can be identified via conventional indentation tests, while an AFM system is quite complicated and expensive. Furthermore, these systems are used

for material identification in laboratories and cannot be used for *in vivo* elasticity imaging. For example, Huth et al. [60] determined the Young's moduli of some hydrogels using AFM indentation tests and the Hertz model. Orikasa et al. [61] introduced an indentation-based testing platform to measure the stiffness of ultra-soft materials at different scales. However, the model proposed by Koruk [54] can be implemented to identify the shear or Young's modulus and viscosity of the tissue. This model can even be used to evaluate the density and Poisson's ratio of the tissue.

Koruk et al. [62] have recently updated the mathematical model in [54] for a trapezoidal pulsed force. Furthermore, Koruk and Pouliopoulos [63] have recently extended the mathematical model for a spherical object placed at the elastic and viscoelastic material interface in [53,54] for different practical loading cases. The mathematical models in [63] simulate the change in the frequency of oscillations of the spherical object located at the medium interface with the applied load. It was shown that the frequencies of oscillations were different in the loading and unloading phases, and the frequency of oscillations decreased with decreasing external load [63]. The shear modulus and viscosity of a gelatin sample with a density of 1133 kg/m^3 were determined to be 6800 Pa and 6.0 Pa·s, respectively [63].

4. Evaluation of Elasticity/Viscoelasticity Imaging Using Particles Located within the Tissue and at the Tissue Interface

4.1. Evaluation of Mathematical Models

Here, we compared the most updated mathematical models for small particles located within the tissue and at the tissue interface and evaluated the models. The radius of the bubbles used in practical ultrasound applications is a few micrometers. The radius of the bubbles and spheres used for material characterization in laboratories mostly ranges from tens of micrometers to a few millimeters (e.g., [21,38]). Therefore, here the results for spherical particles with radii of $R = 3$ and 50 μm were presented. The shear modulus of tissue mostly ranges from a few hundred Pascal to ten thousand Pascal, while it is a few thousand Pascal for most tissues (e.g., [36,64]). For example, the shear modulus, density, and viscosity of the liver are around 2000 Pa [64], 1000 kg/m^3 [65], and 0.5 Pa·s [66], respectively. Here, the analyses were performed for physiologically relevant materials (i.e., G = 2000–6000 Pa, ρ = 1000 kg/m^3, and η = 0.01–1.6 Pa·s). It should be noted that, for all the models presented above, scripts were written using Matlab R2022a (MathWorks, Natick, MA, USA) to find the responses of the small particles located within the tissue and at the tissue interface.

The static force required for a specific normalized displacement (i.e., u/R) for a bubble inside the medium (Equation (1)), a sphere inside the medium (Equation (6)), a bubble located at the material interface (Equation (13)), and a sphere placed at the material interface (Equation (19)) is presented in Figure 3a ($R = 3$ μm) and Figure 3c ($R = 50$ μm). The stiffnesses for the four cases are plotted as a function of the normalized displacement in Figure 3b ($R = 3$ μm) and Figure 3d ($R = 50$ μm). The stiffness of the bubble and sphere inside the material are constant, while the stiffness changes nonlinearly with the displacement of the particles located at the medium interface. This stiffness for a normalized displacement of $\frac{u}{R} = 0.5$ is 0.05, 0.08, 0.19, and 0.28 N/m when $R = 3$ μm and 0.81, 1.37, 3.14, and 4.71 N/m when $R = 50$ μm for the sphere located at the material interface, bubble located at the material interface, bubble inside the sample, and sphere inside the sample, respectively. As the stiffness of the system increases, the force required for a specific displacement increases. The value of the force for a normalized displacement of $\frac{u}{R} = 0.5$ is 0.07, 0.12, 0.28 and 0.42 μN when $R = 3$ μm and 20.35, 34.36, 78.54 and 117.8 μN when $R = 50$ μm for the sphere located at the medium interface, bubble located at the medium interface, bubble inside the medium, and sphere inside the medium, respectively. This clearly shows the order of the external force needed to be applied for a specific particle displacement in different systems.

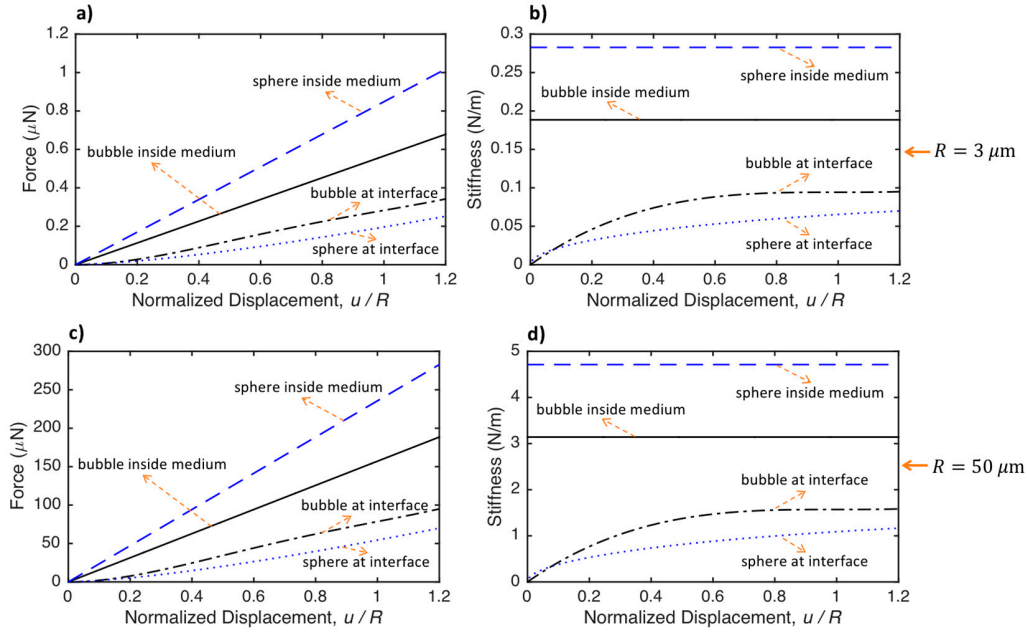

Figure 3. The static force required for a specific normalized displacement (i.e., u/R) for a bubble inside the medium (Equation (1)), a sphere inside the medium (Equation (6)), a bubble located at the medium interface (Equation (13)), and a sphere placed at the material interface (Equation (19)) for $R = 3$ μm (**a**) and $R = 50$ μm (**c**). The stiffnesses for the four cases as a function of the normalized displacement for $R = 3$ μm (**b**) and $R = 50$ μm (**d**). The sample properties are $G = 5000$ Pa and $v = 0.45$. The plots clearly show the stiffnesses and the order of the external force needed to be applied to a specific particle displacement for different systems.

The dynamic responses for a bubble inside the medium (Equation (4)), a sphere inside the medium (Equation (9)), a bubble located at the medium interface (Equation (16)), and a sphere located at the medium interface (Equation (22)) for $R = 3$ μm (a and b) and $R = 50$ μm (c and d) and for two different medium viscosities ($\eta = 0.02$ and 0.2 Pa·s) are presented in Figure 4. Among the four small particles with $R = 3$ μm, only the sphere located at the medium interface oscillates when $\eta = 0.02$ Pa·s. However, this small sphere does oscillate when the viscosity is increased to $\eta = 0.2$ Pa·s. On the other hand, when the particle size is increased (i.e., $R = 50$ μm), both the sphere inside the medium and the sphere located at the medium interface oscillate for the viscosity $\eta = 0.02$ Pa·s. It is seen that this larger sphere located at the sample interface still oscillates for the viscosity $\eta = 0.2$ Pa·s. As expected, the period of oscillations of the particle increases (or the frequency of oscillation decreases) as the size of the particle increases. For instance, the frequencies of oscillations are 38,168 and 2825 Hz for the 3 and 50 μm spheres, respectively, when $\eta = 0.02$ Pa·s. The viscosity has a small effect on the frequency of oscillation. For example, the frequency of oscillations decreases from 2825 to 2674 Hz for the 50 μm sphere placed at the medium interface when the medium viscosity increases from $\eta = 0.02$ to 0.2 Pa·s. The time needed for the particle to reach the steady-state increases as medium viscosity increases. However, the viscosity does not alter the steady-state displacements of the particles.

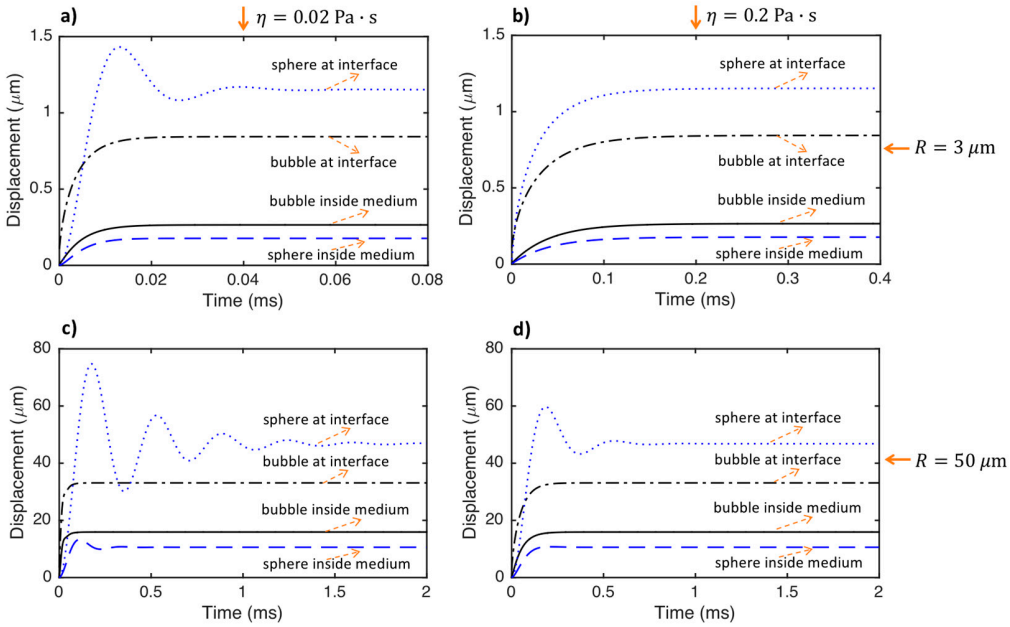

Figure 4. The dynamic responses for a bubble inside the medium (Equation (4)), a sphere inside the medium (Equation (9)), a bubble placed at the material interface (Equation (16)) and a sphere placed at the medium interface (Equation (22)) for $R = 3$ μm and $\eta = 0.02$ Pa·s (**a**) and $\eta = 0.2$ Pa·s (**b**) and for $R = 50$ μm and $\eta = 0.02$ Pa·s (**c**) and $\eta = 0.2$ Pa·s (**d**). The medium properties are $G = 5000$ Pa, $\rho = 1000$ kg/m^3, and $v = 0.45$, and the sphere density is $\rho_s = 9000$ kg/m^3. The force applied to the small and large particles is 0.05 and 50 μN, respectively.

The effects of medium shear modulus and viscosity on the dynamic responses of a bubble inside the medium (Equation (4)), a sphere inside the medium (Equation (9)), a bubble placed at the sample interface (Equation (16)), and a sphere located at the sample interface (Equation (22)) for $R = 50$ μm are presented in Figures 5 and 6, respectively. It is seen that the displacement of the particles decreases as the shear modulus of the sample increases. The particles react faster, and the time to reach the steady-state decreases as the shear modulus of the sample increases and its viscosity decreases. The period of oscillations decreases (or the frequency of oscillation increases) as the material shear modulus increases. Although the displacements of the particles at a specific time before steady-state decrease with increasing medium viscosity, the viscosity does not alter the steady-state displacements of the particles. The mathematical models for all the particles can properly simulate the effects of the shear modulus and viscosity of the medium on the dynamic responses of the particles.

In addition to the time-domain data, the frequency-domain data (spectra) can be used to identify the tissue properties. The FFTs, or Fast Fourier Transforms, of the response of the sphere placed at the sample interface for different medium shear moduli, densities, and viscosities are presented in Figure 7. The spectra clearly show that the displacement of the particle decreases and its frequency of oscillations increases with increasing medium shear modulus. The displacement of the particle and its frequency of oscillations decrease with increasing material density. The displacement of the particle considerably decreases, and its frequency of oscillations slightly decreases with increasing medium viscosity.

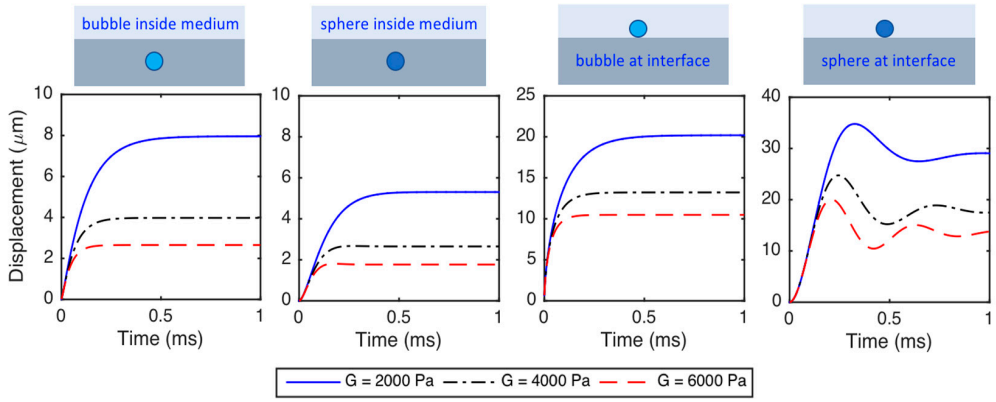

Figure 5. The effect of medium shear modulus on the dynamic responses of a bubble inside the medium (Equation (4)), a sphere inside the medium (Equation (9)), a bubble placed at the material interface (Equation (16)), and a sphere placed at the material interface (Equation (22)) for $R = 50$ μm. The medium properties are $\rho = 1000$ kg/m^3, $\eta = 0.2$ Pa·s, and $v = 0.45$, and the sphere density is $\rho_s = 9000$ kg/m^3. The force applied to the particles is 10 μN.

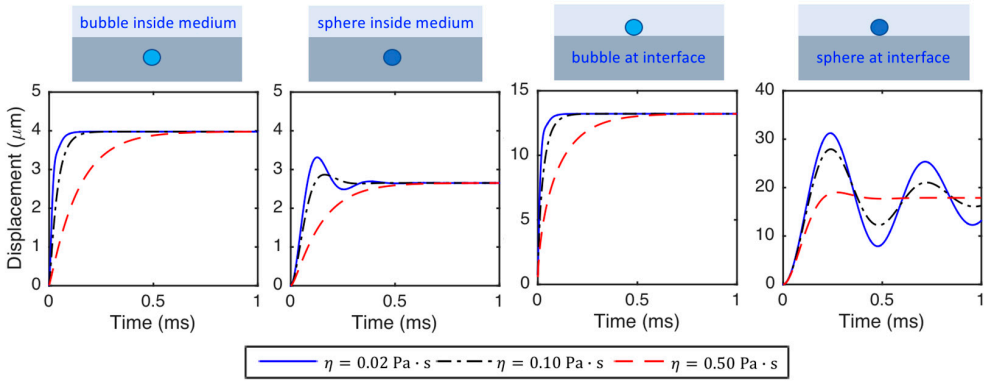

Figure 6. The effect of medium viscosity on the dynamic responses of a bubble inside the medium (Equation (4)), a sphere inside the medium (Equation (9)), a bubble placed at the sample interface (Equation (16)), and a sphere located at the sample interface (Equation (22)) for $R = 50$ μm. The medium properties are $\rho = 1000$ kg/m^3, $G = 4000$ Pa, and $v = 0.45$, and the sphere density is $\rho_s = 9000$ kg/m^3. The force applied to the particles is 10 μN.

In addition to the part of the curve during loading, the part of the curve corresponding to unloading can be used to identify the tissue properties. The external force function and the dynamic responses for a bubble inside the sample (Equation (4)), a sphere inside the sample (Equation (9)), a bubble located at the sample interface (Equation (16)), and a sphere located at the sample interface (Equation (22)) for $R = 3$ μm (a and c) and $R = 50$ μm (b and d) and for two different medium viscosities ($\eta = 0.8$ and 1.6 Pa·s) are presented in Figure 8. It is observed that as the viscosity of the sample increases, the particle's response slows down during loading and unloading. The part of the curve corresponding to loading or unloading can be used to identify medium viscosity. The response rate is lowest for the bubble located at the medium interface, and the response rate is quite high for the sphere placed at the sample interface.

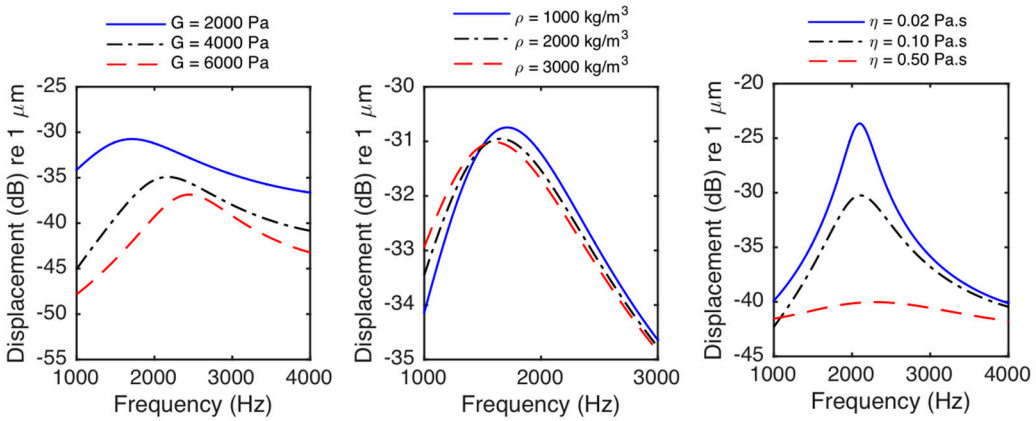

Figure 7. The spectrum of the response of the sphere placed at the sample interface for different medium shear moduli (**left panel**), densities (**center panel**), and viscosities (**right panel**) for $R = 50$ μm. The Poisson's ratio of the sample is $v = 0.45$ and the sphere density is $\rho_s = 9000$ kg/m^3. The force applied to the particle is 10 μN. The medium density and viscosity are $\rho = 1000$ kg/m^3 and $\eta = 0.2$ Pa·s for the left panel. The medium shear modulus and viscosity are $G = 2000$ Pa and $\eta = 0.2$ Pa·s for the center panel. The shear modulus and density of the sample are $G = 4000$ Pa and $\rho = 1000$ kg/m^3 for the right panel.

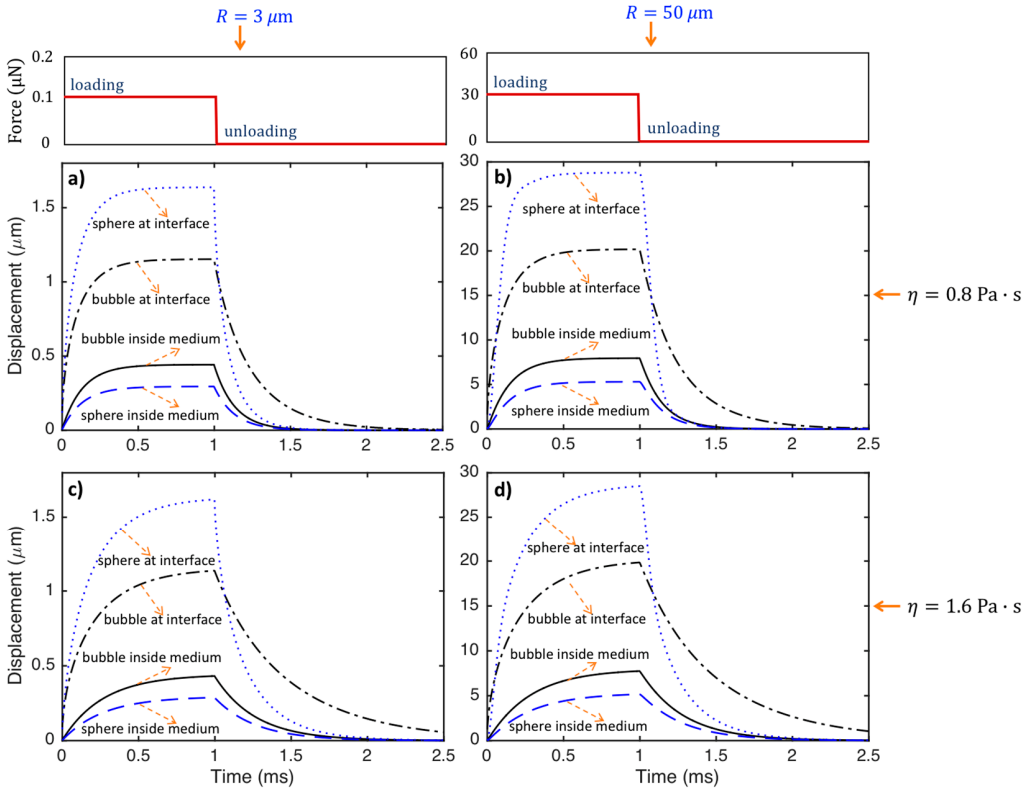

Figure 8. The dynamic responses for a bubble inside the medium (Equation (4)), a sphere inside the medium (Equation (9)), a bubble placed at the sample interface (Equation (16)) and a sphere located at the sample interface (Equation (22)) for $R = 3$ μm (**a**,**c**) and $R = 50$ μm (**b**,**d**) and for medium viscosities $\eta = 0.8$ (**a**,**b**) and 1.6 Pa·s (**c**,**d**). The medium properties are $G = 6000$ Pa, $\rho = 1000$ kg/m^3, and $v = 0.45$, and the sphere density is $\rho_s = 9000$ kg/m^3. The force applied to the small and large particles is 0.1 and 30 μN, respectively.

The displacement u presented so far shows the displacement of the tip point (the tip contact point between the particle and medium). It should be noted that displacement u is mostly used for elasticity and viscoelastic imaging purposes. However, if it is needed,

the radial $u_r(r,\theta)$ and polar $u_\theta(r,\theta)$ displacement components and radial $\sigma_r(r,\theta)$ and polar $\sigma_\theta(r,\theta)$ stress components at every point of the medium can be determined (see Figure 2b). Readers may refer to the references [19,33] for the corresponding displacement and stress expressions for a bubble and sphere inside the medium. Readers may refer to the references [33,46] for a bubble located at the sample interface and to the reference [33] for the sphere placed at the sample interface for the corresponding displacement and stress expressions.

4.2. Evaluation of Tissue Identification Systems

Some of the elasticity and viscoelasticity imaging studies based on measurements and the mathematical models presented above are summarized in Table 1. Ultrasonic excitation and monitoring are mostly used to identify material properties, though magnetic and mechanical excitation and optical and MRI imaging can be used for elasticity and viscoelastic imaging based on the use of small particles located within the tissue and at the tissue interface (see Figure 2a). It is seen that there are still no applications for the *in vivo* identification of tissue properties based on the use of small particles located within the tissue and at the tissue interface. Although the particles inside the tissue have been used for the last 70 years, this technique uses a high-powered laser to create the bubble inside the medium. This restricts its application to shallow targets and demands local destruction of the material. A bubble (or a non-deformable sphere) must be placed inside the tissue, which may not be permissible in human tissue (e.g., [20,43]). However, owing to the mathematical models recently proposed for the particles located at the tissue interfaces [46,47,53,54,62,63], it is believed that *in vivo* tissue identification can be possible in the future. We believe that tissue identification based on small particles located within the tissue and at the tissue interface has the potential to change the field, as they can provide the determination of accurate and local tissue elastic properties as well as density, Poisson's ratio, and viscosity, thanks to the sophisticated mathematical models developed. We propose the use of the term viscoelasticity imaging, as unlike conventional elasticity imaging, which maps the elastic properties of the tissue, some other properties of the tissue, such as its viscosity, can be identified using particle-mediated imaging methods.

As mentioned before, because there is a need to locate the particles inside the medium to be able to use mathematical models, these models are even more difficult to use for the identification of tissue-mimicking materials or *ex vivo* tissue in the laboratory. However, as it is straightforward to locate a particle at the medium interface and this does not alter material properties, the mathematical models for the particles located at the medium interface can be easily used for the identification of material properties of tissue-mimicking materials and *ex vivo* tissue in the laboratory. In addition to the elastic properties of the medium and size of the sphere, the model for the sphere placed at the material interface includes the corrected models for the inertia force due to the sample involved in motion, the inertia force of the sphere, and the damping due to the sphere oscillations arising from the radiation of shear waves. Furthermore, the force-displacement relation is valid for the small and large displacements of the sphere and the practical values of the medium Poisson's ratio and the experimental setup is very straightforward. Therefore, this system seems very promising for tissue identification purposes.

Table 1. Some of the elasticity and viscoelasticity imaging studies.

Particle Used	Particle Location	Excitation Method	Monitoring Method	Target Material	Identified Property	Reference
bubble	inside medium	ultrasonic	ultrasonic	gelation phantom	Young's modulus	Erpelding et al., 2005 [20]
bubble	inside medium	ultrasonic	ultrasonic	human lenses	Young's modulus	Hollman et al., 2007 [35]
bubble	inside medium	ultrasonic	ultrasonic	bovine and porcine crystalline lenses	Young's modulus and viscosity	Yoon et al., 2013 [39]
sphere	inside medium	ultrasonic	ultrasonic	gelation phantom	shear modulus	Karpiouk et al., 2009 [41]
sphere	inside medium	ultrasonic	ultrasonic	porcine blood clots	shear modulus and viscosity	Huang et al., 2011 [43]
sphere	inside medium	magnetic	ultrasonic	gelation phantom	shear modulus and viscosity	Cebrecos et al., 2021 [45]
cloud of bubbles	at a medium interface	ultrasonic	optical	gelation phantom	shear modulus	Koruk et al., 2015 [23]
bubble	at a medium interface	ultrasonic	optical	hydrogel	shear modulus and viscosity	Bezer et al., 2020 [24]
sphere	at a medium interface	magnetic	optical	gelation phantom	shear modulus and viscous damping ratio	Koruk et al., 2022 [55]
sphere	at a medium interface	magnetic	optical	gelation phantom	shear modulus and viscosity	Koruk et al., 2022 [62]; Koruk and Pouliopoulos [63]

The mathematical models presented in this paper can be used to identify material properties on macroscopic or microscopic scales. If only the identification of the Young's modulus (or shear modulus) of the tissue is required (i.e., elasticity imaging), it is only needed to measure the displacement of the particle exposed to a static force or the steady-state displacement of the particle exposed to a dynamic force. Using the corresponding mathematical models for a static external force (i.e., Equations (1), (6), (13) or (19)), the elastic properties of the tissue can be identified. However, besides the elasticity or shear modulus, if the identification of the density and/or viscosity of tissue is required (i.e., viscoelasticity imaging), there is a need to measure the dynamic response of the particle and to use the corresponding mathematical models for dynamic loading (i.e., Equations (4), (9), (16), or (22)). By performing curve fitting using experimental data and mathematical models, the elasticity modulus, density, and viscosity of the tissue can be identified. Alternatively, the elastic properties can be determined from the steady-state displacement, the viscosity can be identified from the part of the measured curve corresponding to loading or unloading, and the density of the tissue can be determined by matching the measured and theoretical oscillating frequency of the particle. Furthermore, it may be difficult to know the magnitude of the applied force. In practice, without needing the amplitude of the applied force, the elasticity or shear modulus and/or the density of tissue can be identified by matching the measured and theoretical oscillating frequency of the particle, and the viscosity of tissue can be identified from the part of the measured curve corresponding to loading or unloading. In addition, the frequency of oscillation of the particle and damping of tissue can be determined using the spectrum of the time-domain data and the modal analysis techniques, such as half-power, circle-fit, or line-fit (e.g., [67]).

5. Concluding Remarks

In this paper, we investigated the elasticity/viscoelasticity imaging based on the use of small particles located within the tissue and at the tissue interface exposed to static and dynamic external loads. We compared the mathematical models for the small particles exposed to static and dynamic external loads and evaluated the elasticity and viscoelasticity imaging methods based on the use of small particles located within the tissue and at the tissue interface. Some concluding remarks are presented below.

The acoustic radiation force-based elasticity imaging techniques that remotely palpate material produce a complicated displacement field. The displacement field depends on the transducer's focusing properties and target geometry. For the absorption-based techniques, the focal volume influences elasticity reconstruction. For elasticity imaging based on the use of small particles located within the tissue and at the tissue interface, particle displacement is independent of the focal zone of the transducer and is affected only by the viscoelastic properties of the local tissue, and simple and accurate elasticity reconstruction can be performed. As sophisticated mathematical models for a particle located within the tissue and at the tissue interface can be developed, in addition to elastic properties, density and viscosity of tissue can be determined in particle-mediated elasticity imaging.

Because the radiation force exerted on the particle located within the tissue and at the tissue interface is normally far greater than that occurring in a purely absorbing medium, a lower acoustic power can be used in a moderately attenuating medium for particle-mediated elasticity imaging techniques. For the particles located inside the tissue, there is a need to use a high-powered laser to create the bubble inside the medium, which restricts its application to shallow targets and demands local destruction of the material, or there is a need to position a bubble (or rigid sphere) inside the tissue. This may not be permissible in human tissue. However, exploiting the models recently proposed for the particles located at the tissue interfaces, it is believed that *in vivo* tissue identification can be possible in the future. Furthermore, using the well-established mathematical models, the particles located at the medium interface can be conveniently used to identify tissue-mimicking materials and *ex vivo* tissue in the laboratory.

The stiffness of the bubble and sphere inside the medium is constant, while the stiffness varies nonlinearly with the displacement of the particles located at the medium interfaces. The stiffness, hence the force required for a specific displacement of the particle, increases from the sphere placed at the material interface to the bubble located at the material interface, the bubble inside the medium, and the sphere inside the sample. The value of force needed for a ratio of 0.5 particle displacement to the radius of the special object and a medium with a shear modulus of 5000 Pa is around 70–420 nano Newton and 20–120 micro-Newton for particles with a radius of 3 and 50 μm, respectively.

The period of oscillations of the particle significantly increases (or the frequency of oscillation significantly decreases) as the size of the particle increases. However, even the spherical object placed at the sample interface does not have any oscillations if the particle size is small and the material viscosity is considerably high. The displacement of the particles decreases as the medium shear modulus increases. The particles react faster, and the time to reach the steady-state decreases as the shear modulus of the sample increases. The period of oscillations decreases (or the frequency of oscillation increases) as the material shear modulus increases. The displacements of the particles at a specific time before steady-state decrease with increasing sample viscosity. The particles react faster, and the time needed for the particle to reach the steady-state decreases as medium viscosity decreases. The viscosity does not alter the steady-state displacements of the particles. The frequency of oscillation of the particle interacting with tissue slightly decreases as sample viscosity increases. The frequency of oscillations of the particle interacting with tissue decreases with increasing medium density.

If only the identification of the Young's modulus (or shear modulus) of the tissue is required (i.e., elasticity imaging), it is only needed to measure the displacement of the particle exposed to a static force or the steady-state displacement of the particle exposed

to a dynamic force. Using the corresponding mathematical models for a static external force, the elastic properties of the tissue can be identified. However, in addition to the elasticity or shear modulus, if the identification of the density and/or viscosity of the tissue is required (i.e., viscoelasticity imaging), there is a need to measure the dynamic response of the particle and to use the corresponding mathematical models for dynamic loading. By performing curve fitting using experimental data and mathematical models, the Young's (or shear) modulus, density, and viscosity of the tissue can be identified. Alternatively, the elastic properties can be determined from the steady-state displacement, the viscosity can be identified from the part of the measured curve corresponding to loading or unloading, and the density of the tissue can be determined by matching the measured and theoretical oscillating frequency of the particle. Furthermore, as it may be difficult to know the magnitude of the exerted force in practice, without needing the amplitude of the applied force, the Young's modulus (or shear) modulus and/or the density of the tissue can be identified by matching the measured and theoretical oscillating frequency of the particle, and the viscosity of the tissue can be identified from the part of the measured curve corresponding to loading or unloading.

Although ultrasonic excitation and monitoring are mostly used to identify material properties based on small particles, magnetic and mechanical excitation and optical and MRI imaging can be used for elasticity and viscoelastic imaging based on small particles. We believe that tissue identification based on the use of small particles located within the tissue and at the tissue interface has the potential to change the field, as they can provide the determination of accurate and local tissue elastic properties as well as density, Poisson's ratio, and viscosity, owing to the sophisticated mathematical models developed. We suggest the use of the term viscoelasticity imaging, as unlike traditional elasticity imaging, which maps the elastic properties of the tissue, some other properties of the tissue, such as its viscosity, can be determined using particle-mediated imaging methods.

Author Contributions: Conceptualization, H.K.; Methodology, H.K.; Software, H.K.; Validation, H.K.; Formal Analysis, H.K.; Investigation, H.K. and A.N.P.; Resources, H.K. and A.N.P.; Data Curation, H.K.; Writing–Original Draft Preparation, H.K.; Writing–Review & Editing, H.K. and A.N.P.; Visualization, H.K. and A.N.P.; Supervision, H.K. and A.N.P.; Project Administration, H.K. and A.N.P.; Funding Acquisition, H.K. and A.N.P. All authors have read and agreed to the published version of the manuscript.

Funding: Hasan Koruk was supported by the Focused Ultrasound Foundation (grant number FUS1050R1) and the Little Princess Trust (grant number CCLGA 2022-2025).

Data Availability Statement: Data are contained within the article.

Conflicts of Interest: The authors declare no conflict of interest.

References

1. Konofagou, E.E. Quo Vadis Elasticity Imaging? *Ultrasonics* **2004**, *42*, 331–336. [CrossRef]
2. Manduca, A.; Oliphant, T.E.; Dresner, M.A.; Mahowald, J.L.; Kruse, S.A.; Amromin, E.; Felmlee, J.P.; Greenleaf, J.F.; Ehman, R.L. Magnetic Resonance Elastography: Non-Invasive Mapping of Tissue Elasticity. *Med. Image Anal.* **2001**, *5*, 237–254. [CrossRef] [PubMed]
3. Lee, S.; Eun, L.Y.; Hwang, J.Y.; Eun, Y. Ex Vivo Evaluation of Mechanical Anisotropic Tissues with High-Frequency Ultrasound Shear Wave Elastography. *Sensors* **2022**, *22*, 978. [CrossRef] [PubMed]
4. Ličen, U.; Kozinc, Ž. Using Shear-Wave Elastography to Assess Exercise-Induced Muscle Damage: A Review. *Sensors* **2022**, *22*, 7574. [CrossRef]
5. Mostafa, F.; Greenleaf, J.F. Ultrasound-Stimulated Vibro-Acoustic Spectrography. *Science* **1998**, *280*, 82–85. [CrossRef]
6. Sarvazyan, A.P.; Rudenko, O.V.; Swanson, S.D.; Fowlkes, J.B.; Emelianov, S.Y. Shear Wave Elasticity Imaging: A New Ultrasonic Technology of Medical Diagnostics. *Ultrasound Med. Biol.* **1998**, *24*, 1419–1435. [CrossRef] [PubMed]
7. Nightingale, K.R.; Palmeri, M.L.; Nightingale, R.W.; Trahey, G.E. On the Feasibility of Remote Palpation Using Acoustic Radiation Force. *J. Acoust. Soc. Am.* **2001**, *110*, 625–634. [CrossRef] [PubMed]
8. Konofagou, E.E.; Hynynen, K. Localized Harmonic Motion Imaging: Theory, Simulations and Experiments. *Ultrasound Med. Biol.* **2003**, *29*, 1405–1413. [CrossRef]

9. Bercoff, J.; Tanter, M.; Fink, M. Supersonic Shear Imaging: A New Technique for Soft Tissue Elasticity Mapping. *IEEE Trans. Ultrason. Ferroelectr. Freq. Control* **2004**, *51*, 396–409. [CrossRef]
10. Deffieux, T.; Montaldo, G.; Tanter, M.; Fink, M. Shear Wave Spectroscopy for in Vivo Quantification of Human Soft Tissues Visco-Elasticity. *IEEE Trans. Med. Imaging* **2009**, *28*, 313–322. [CrossRef]
11. Palmeri, M.L.; Nightingale, K.R. Acoustic Radiation Force-Based Elasticity Imaging Methods. *Interface Focus* **2011**, *1*, 553–564. [CrossRef] [PubMed]
12. Doherty, J.; Trahey, G.; Nightingale, K.; Palmeri, M. Acoustic Radiation Force Elasticity Imaging in Diagnostic Ultrasound. *IEEE Trans. Ultrason. Ferroelectr. Freq. Control* **2013**, *60*, 685–701. [CrossRef] [PubMed]
13. Shiina, T.; Nightingale, K.R.; Palmeri, M.L.; Hall, T.J.; Bamber, J.C.; Barr, R.G.; Castera, L.; Choi, B.I.; Chou, Y.-H.; Cosgrove, D.; et al. WFUMB Guidelines and Recommendations for Clinical Use of Ultrasound Elastography: Part 1: Basic Principles and Terminology. *Ultrasound Med. Biol.* **2015**, *41*, 1126–1147. [CrossRef] [PubMed]
14. Barr, R.G.; Nakashima, K.; Amy, D.; Cosgrove, D.; Farrokh, A.; Schafer, F.; Bamber, J.C.; Castera, L.; Choi, B.I.; Chou, Y.-H.; et al. WFUMB Guidelines and Recommendations for Clinical Use of Ultrasound Elastography: Part 2: Breast. *Ultrasound Med. Biol.* **2015**, *41*, 1148–1160. [CrossRef] [PubMed]
15. Ferraioli, G.; Filice, C.; Castera, L.; Choi, B.I.; Sporea, I.; Wilson, S.R.; Cosgrove, D.; Dietrich, C.F.; Amy, D.; Bamber, J.C.; et al. WFUMB Guidelines and Recommendations for Clinical Use of Ultrasound Elastography: Part 3: Liver. *Ultrasound Med. Biol.* **2015**, *41*, 1161–1179. [CrossRef] [PubMed]
16. Cosgrove, D.; Barr, R.; Bojunga, J.; Cantisani, V.; Chammas, M.C.; Dighe, M.; Vinayak, S.; Xu, J.-M.; Dietrich, C.F. WFUMB Guidelines and Recommendations on the Clinical Use of Ultrasound Elastography: Part 4. Thyroid. *Ultrasound Med. Biol.* **2017**, *43*, 4–26. [CrossRef] [PubMed]
17. Barr, R.G.; Cosgrove, D.; Brock, M.; Cantisani, V.; Correas, J.M.; Postema, A.W.; Salomon, G.; Tsutsumi, M.; Xu, H.-X.; Dietrich, C.F. WFUMB Guidelines and Recommendations on the Clinical Use of Ultrasound Elastography: Part 5. Prostate. *Ultrasound Med. Biol.* **2017**, *43*, 27–48. [CrossRef]
18. Chen, S.; Fatemi, M.; Greenleaf, J.F. Remote Measurement of Material Properties from Radiation Force Induced Vibration of an Embedded Sphere. *J. Acoust. Soc. Am.* **2002**, *112*, 884–889. [CrossRef]
19. Ilinskii, Y.A.; Meegan, G.D.; Zabolotskaya, E.A.; Emelianov, S.Y. Gas Bubble and Solid Sphere Motion in Elastic Media in Response to Acoustic Radiation Force. *J. Acoust. Soc. Am.* **2005**, *117*, 2338–2346. [CrossRef]
20. Erpelding, T.N.; Hollman, K.W.; O'Donnell, M. Bubble-Based Acoustic Radiation Force Elasticity Imaging. *IEEE Trans. Ultrason. Ferroelectr. Freq. Control* **2005**, *52*, 971–979. [CrossRef]
21. Aglyamov, S.R.; Karpiouk, A.B.; Ilinskii, Y.A.; Zabolotskaya, E.A.; Emelianov, S.Y. Motion of a Solid Sphere in a Viscoelastic Medium in Response to Applied Acoustic Radiation Force: Theoretical Analysis and Experimental Verification. *J. Acoust. Soc. Am.* **2007**, *122*, 1927–1936. [CrossRef]
22. Urban, M.W.; Nenadic, I.Z.; Mitchell, S.A.; Chen, S.; Greenleaf, J.F. Generalized Response of a Sphere Embedded in a Viscoelastic Medium Excited by an Ultrasonic Radiation Force. *J. Acoust. Soc. Am.* **2011**, *130*, 1133–1141. [CrossRef] [PubMed]
23. Koruk, H.; El Ghamrawy, A.; Pouliopoulos, A.N.; Choi, J.J. Acoustic Particle Palpation for Measuring Tissue Elasticity. *Appl. Phys. Lett.* **2015**, *107*, 223701. [CrossRef]
24. Bezer, J.H.; Koruk, H.; Rowlands, C.J.; Choi, J.J. Elastic Deformation of Soft Tissue-Mimicking Materials Using a Single Microbubble and Acoustic Radiation Force. *Ultrasound Med. Biol.* **2020**, *46*, 3327–3338. [CrossRef] [PubMed]
25. Rus, G.; Faris, I.H.; Torres, J.; Callejas, A.; Melchor, J. Why Are Viscosity and Nonlinearity Bound to Make an Impact in Clinical Elastographic Diagnosis? *Sensors* **2020**, *20*, 2379. [CrossRef] [PubMed]
26. Nightingale, K.; Soo, M.S.; Nightingale, R.; Trahey, G. Acoustic Radiation Force Impulse Imaging: In Vivo Demonstration of Clinical Feasibility. *Ultrasound Med. Biol.* **2002**, *28*, 227–235. [CrossRef]
27. Fatemi, M.; Greenleaf, J.F. Vibro-Acoustography: An Imaging Modality Based on Ultrasound-Stimulated Acoustic Emission. *Proc. Natl. Acad. Sci. USA* **1999**, *96*, 6603–6608. [CrossRef] [PubMed]
28. Yang, X.; Church, C.C. A Model for the Dynamics of Gas Bubbles in Soft Tissue. *J. Acoust. Soc. Am.* **2005**, *118*, 3595–3606. [CrossRef]
29. Zabolotskaya, E.A.; Ilinskii, Y.A.; Meegan, G.D.; Hamilton, M.F. Modifications of the Equation for Gas Bubble Dynamics in a Soft Elastic Medium. *J. Acoust. Soc. Am.* **2005**, *118*, 2173–2181. [CrossRef]
30. Barajas, C.; Johnsen, E. The Effects of Heat and Mass Diffusion on Freely Oscillating Bubbles in a Viscoelastic, Tissue-like Medium. *J. Acoust. Soc. Am.* **2017**, *141*, 908–918. [CrossRef]
31. Hamaguchi, F.; Ando, K. Linear Oscillation of Gas Bubbles in a Viscoelastic Material under Ultrasound Irradiation. *Phys. Fluids* **2015**, *27*, 113103. [CrossRef]
32. Landau, L.D.; Lifshitz, E.M. *Fluid Mechanics*, 2nd ed.; Pergamon: New York, NY, USA, 1987.
33. Koruk, H. Assessment of the Models for Predicting the Responses of Spherical Objects in Viscoelastic Mediums and at Viscoelastic Interfaces. *IOP Conf. Ser. Mater. Sci. Eng.* **2021**, *1150*, 012016. [CrossRef]
34. Erpelding, T.N.; Hollman, K.W.; O'Donnell, M. Mapping Age-Related Elasticity Changes in Porcine Lenses Using Bubble-Based Acoustic Radiation Force. *Exp. Eye Res.* **2007**, *84*, 332–341. [CrossRef] [PubMed]
35. Hollman, K.W.; O'Donnell, M.; Erpelding, T.N. Mapping Elasticity in Human Lenses Using Bubble-Based Acoustic Radiation Force. *Exp. Eye Res.* **2007**, *85*, 890–893. [CrossRef] [PubMed]

36. Mikula, E.; Hollman, K.; Chai, D.; Jester, J.V.; Juhasz, T. Measurement of Corneal Elasticity with an Acoustic Radiation Force Elasticity Microscope. *Ultrasound Med. Biol.* **2014**, *40*, 1671–1679. [CrossRef] [PubMed]
37. Mikula, E.R.; Jester, J.V.; Juhasz, T. Measurement of an Elasticity Map in the Human Cornea. *Investig. Ophthalmol. Vis. Sci.* **2016**, *57*, 3282–3286. [CrossRef] [PubMed]
38. Yoon, S.; Aglyamov, S.R.; Karpiouk, A.B.; Kim, S.; Emelianov, S.Y. Estimation of Mechanical Properties of a Viscoelastic Medium Using a Laser-Induced Microbubble Interrogated by an Acoustic Radiation Force. *J. Acoust. Soc. Am.* **2011**, *130*, 2241–2248. [CrossRef] [PubMed]
39. Yoon, S.; Aglyamov, S.; Karpiouk, A.; Emelianov, S. The Mechanical Properties of Ex Vivo Bovine and Porcine Crystalline Lenses: Age-Related Changes and Location-Dependent Variations. *Ultrasound Med. Biol.* **2013**, *39*, 1120–1127. [CrossRef]
40. Oestreicher, H.L. Field and Impedance of an Oscillating Sphere in a Viscoelastic Medium with an Application to Biophysics. *J. Acoust. Soc. Am.* **1951**, *23*, 707–714. [CrossRef]
41. Karpiouk, A.B.; Aglyamov, S.R.; Ilinskii, Y.A.; Zabolotskaya, E.A.; Emelianov, S.Y. Assessment of Shear Modulus of Tissue Using Ultrasound Radiation Force Acting on a Spherical Acoustic Inhomogeneity. *IEEE Trans. Ultrason. Ferroelectr. Freq. Control* **2009**, *56*, 2380–2387. [CrossRef]
42. Shih, C.; Liu, T.; Huang, C. In Vitro Assessments of Viscoelastic Properties of Fibrin Clot by Using Acoustic Radiation Force on a Solid Sphere. In Proceedings of the 2010 IEEE International Ultrasonics Symposium, San Diego, CA, USA, 11–14 October 2010; pp. 479–482.
43. Huang, C.-C.; Shih, C.-C.; Liu, T.-Y.; Lee, P.-Y. Assessing the Viscoelastic Properties of Thrombus Using a Solid-Sphere-Based Instantaneous Force Approach. *Ultrasound Med. Biol.* **2011**, *37*, 1722–1733. [CrossRef] [PubMed]
44. Levy, B.E.; Oldenburg, A.L. Single Magnetic Particle Motion in Magnetomotive Ultrasound: An Analytical Model and Experimental Validation. *IEEE Trans. Ultrason. Ferroelectr. Freq. Control* **2021**, *68*, 2635–2644. [CrossRef] [PubMed]
45. Cebrecos, A.; Jiménez, N.; Tarazona, R.; Company, M.; Benlloch, J.M.; Camarena, F. Characterization of Viscoelastic Media Combining Ultrasound and Magnetic-Force Induced Vibrations on an Embedded Soft Magnetic Sphere. *IEEE Trans. Ultrason. Ferroelectr. Freq. Control* **2021**, *68*, 3540–3548. [CrossRef] [PubMed]
46. Koruk, H.; Choi, J.J. Displacement of a Bubble by Acoustic Radiation Force into a Fluid–Tissue Interface. *J. Acoust. Soc. Am.* **2018**, *143*, 2535–2540. [CrossRef] [PubMed]
47. Koruk, H.; Choi, J.J. Displacement of a Bubble Located at a Fluid-Viscoelastic Medium Interface. *J. Acoust. Soc. Am.* **2019**, *145*, EL410–EL416. [CrossRef] [PubMed]
48. Wu, C.-E.; Lin, K.-H.; Juang, J.-Y. Hertzian Load–Displacement Relation Holds for Spherical Indentation on Soft Elastic Solids Undergoing Large Deformations. *Tribol. Int.* **2016**, *97*, 71–76. [CrossRef]
49. Sneddon, I.N. The Relation between Load and Penetration in the Axisymmetric Boussinesq Problem for a Punch of Arbitrary Profile. *Int. J. Eng. Sci.* **1965**, *3*, 47–57. [CrossRef]
50. Dimitriadis, E.K.; Horkay, F.; Maresca, J.; Kachar, B.; Chadwick, R.S. Determination of Elastic Moduli of Thin Layers of Soft Material Using the Atomic Force Microscope. *Biophys. J.* **2002**, *82*, 2798–2810. [CrossRef]
51. Guo, Z.; Hao, M.; Jiang, L.; Li, D.; Chen, Y.; Dong, L. A Modified Hertz Model for Finite Spherical Indentation Inspired by Numerical Simulations. *Eur. J. Mech. A/Solids* **2020**, *83*, 104042. [CrossRef]
52. Kontomaris, S.V.; Malamou, A. A Novel Approximate Method to Calculate the Force Applied on an Elastic Half Space by a Rigid Sphere. *Eur. J. Phys.* **2021**, *42*, 25010. [CrossRef]
53. Koruk, H. Modelling Small and Large Displacements of a Sphere on an Elastic Half-Space Exposed to a Dynamic Force. *Eur. J. Phys.* **2021**, *52*, 055006. [CrossRef]
54. Koruk, H. Development of an Improved Mathematical Model for the Dynamic Response of a Sphere Located at a Viscoelastic Medium Interface. *Eur. J. Phys.* **2022**, *43*, 25002. [CrossRef]
55. Koruk, H.; Yurdaer, S.B.; Koc, H.O.; Besli, A. Identification of the Viscoelastic Properties of Soft Materials Using a Convenient Dynamic Indentation System and Procedure. *Mater. Today Proc.* **2022**, *57*, 464–468. [CrossRef]
56. Koruk, H.; Besli, A.; Koc, H.O.; Yurdaer, S.B. Identification of Material Viscoelastic Properties Using the Motion of a Rigid Sphere Located at Tissue-Mimicking Material Interface in Response to a Dynamic Force. *Mater. Sci. Forum* **2022**, *1066*, 73–78. [CrossRef]
57. Qiang, B.; Greenleaf, J.; Oyen, M.; Zhang, X. Estimating Material Elasticity by Spherical Indentation Load-Relaxation Tests on Viscoelastic Samples of Finite Thickness. *IEEE Trans. Ultrason. Ferroelectr. Freq. Control* **2011**, *58*, 1418–1429. [CrossRef] [PubMed]
58. Boots, J.N.M.; Fokkink, R.; van der Gucht, J.; Kodger, T.E. Development of a Multi-Position Indentation Setup: Mapping Soft and Patternable Heterogeneously Crosslinked Polymer Networks. *Rev. Sci. Instrum.* **2019**, *90*, 15108. [CrossRef]
59. Chim, Y.H.; Mason, L.M.; Rath, N.; Olson, M.F.; Tassieri, M.; Yin, H. A One-Step Procedure to Probe the Viscoelastic Properties of Cells by Atomic Force Microscopy. *Sci. Rep.* **2018**, *8*, 14462. [CrossRef] [PubMed]
60. Huth, S.; Sindt, S.; Selhuber-Unkel, C. Automated Analysis of Soft Hydrogel Microindentation: Impact of Various Indentation Parameters on the Measurement of Young's Modulus. *PLoS ONE* **2019**, *14*, e0220281. [CrossRef]
61. Orikasa, K.; Bacca, N.; Agarwal, A. Meso/Macro-Scale Ultra-Soft Materials' Mechanical Property Evaluation Device and Testbed. *Rev. Sci. Instrum.* **2021**, *92*, 73904. [CrossRef]
62. Koruk, H.; Koc, H.O.; Yurdaer, S.B.; Besli, A.; Pouliopoulos, A.N. A New Approach for Measuring Viscoelastic Properties of Soft Materials Using the Dynamic Response of a Spherical Object Placed at the Sample Interface. *Exp. Mech.* **2023**. [CrossRef]

63. Koruk, H.; Pouliopoulos, A.N. Investigation of the Motion of a Spherical Object Located at Soft Elastic and Viscoelastic Material Interface for Identification of Material Properties. *Appl. Sci. Eng. Prog.* **2024**, *17*, 7277.
64. Maccabi, A.; Shin, A.; Namiri, N.K.; Bajwa, N.; St. John, M.; Taylor, Z.D.; Grundfest, W.; Saddik, G.N. Quantitative Characterization of Viscoelastic Behavior in Tissue-Mimicking Phantoms and Ex Vivo Animal Tissues. *PLoS ONE* **2018**, *13*, e0191919. [CrossRef] [PubMed]
65. Woodard, H.Q.; White, D.R. The Composition of Body Tissues. *Br. J. Radiol.* **1986**, *59*, 1209–1218. [CrossRef] [PubMed]
66. Chen, S.; Urban, M.W.; Pislaru, C.; Kinnick, R.; Zheng, Y.; Yao, A.; Greenleaf, J.F. Shearwave Dispersion Ultrasound Vibrometry (SDUV) for Measuring Tissue Elasticity and Viscosity. *IEEE Trans. Ultrason. Ferroelectr. Freq. Control* **2009**, *56*, 55–62. [CrossRef]
67. Ewins, D.J. *Modal Testing: Theory, Practice and Application*, 2nd ed.; Research Studies Press Ltd.: Somerset, UK, 2009.